J. Electrochem. Sci. Eng. **13(5)** (2023) 1027-1035; http://dx.doi.org/10.5599/jese.1931

Open Access : : ISSN 1847-9286
https://pub.iapchem.org/ojs/index.php/JESE

Original scientific paper

Comparative corrosion behavior of Au_{50}-Ag_{25}-Pd_{25} and $Ni_{88.6}$-$Cr_{11.4}$ alloys utilized in dental applications

Irfan Liaquat[1,✉], Amer Bashir Ziya[1], Warda Mushtaq[1], Athar Ibrahim[2], Urva Malik[2], Gao Qilong[3] and Muhammad Danial[4]

[1]*Institute of Physics, Bahauddin Zakariya University, Multan-60800, Pakistan*
[2]*Department of Metallurgical Engineering and Materials Science, University of Engineering and Technology, Lahore, Pakistan*
[3]*School of Physical and Microelectronics Zhengzhou University, Zhengzhou 450001, China*
[4]*Department of Physics, University of Education, Lahore, Pakistan*

Corresponding author: ✉irfanliaquat099@gmail.com

Received: June 8, 2023; Accepted: July 26, 2023; Published: July 29, 2023

Abstract

The electrochemical behaviour of alloys (Au_{50}-Ag_{25}-Pd_{25} and $Ni_{88.6}$-$Cr_{11.4}$) was studied in Fusayama's artificial saliva at pH 6.5 and 37 °C by using open circuit potential, electrochemical impedance spectroscopy, and potentiodynamic polarization measurements. Electrochemical impedance spectroscopy results were simulated with an equivalent electrical circuit. After immersion in artificial saliva, surface characterization of samples was done using scanning electron microscopy connected with energy-dispersive spectroscopy. All obtained results revealed that Au_{50}-Ag_{25}-Pd_{25} alloy is much more resistive than $Ni_{88.6}$-$Cr_{11.4}$ and can be recommended for the effective treatment of patients with dental prosthetics that have metal frameworks.

Keywords

Dental alloys; gold-silver-palladium; nickel-chromium; corrosion; electrochemical tests; surface morphology

Introduction

In the history of dental alloys, precious and non-precious metals such as Au, Ni, Cr, Co, Ag, and Pd have often been preferred because of their favorable mechanical as well as biological properties [1]. A special preference in research is reserved for gold (Au) alloys because of their high mechanical effects, low corrosion rate, and superb biocompatibility [2]. Nevertheless, O'Brian and German [3] suggested that the formation of a second phase would increase the corrosion rate of Au-Ag-Cu ternary alloys. German *et al*. [4] suggested that nobility determines the corrosion resistance of gold-based alloys, but alloying with Cu induces silver segregation, causing a lower corrosion rate. Some researchers, however, have used non-precious dental alloys instead of gold

alloys to reduce costs [5-8]. Ni–Cr alloys are also utilized as a substitute for noble dental alloys due to their poor cost and low corrosion rate [9]. However, the biological material of Ni-based alloys in a mouth environment causes several problems owing to allergic reactions to Ni ions. By adding different elements, the microstructure of Ni-based alloys and their properties can be modified. Thus, Cr is commonly used to form a barrier, such that microstructures containing a Cr-rich oxide layer prevent the release of Ni ions from alloys. In general, Ni-Cr casting alloy shows a homogeneous structure but low corrosion resistance. If a small amount of Be element is added to a Ni-based casting alloy, the structure becomes non-homogenous, but corrosion resistance increases [10-12]. The corrosion resistance of Ni-Cr alloys depends on their composition and the formation of a passive oxide film. Experimental studies revealed that alloys with 16 to 27 % Cr form a protective oxide film on the surface and show a low corrosion rate [13]. Commonly, the purpose of the protective oxide film is to act as an obstacle to the flow of electrons within the metal and the electrolyte [14].

The objective of this research is to compare the decomposition rate of precious Au_{50}-Ag_{25}-Pd_{25} alloy with that of non-precious $Ni_{88.6}$-$Cr_{11.4}$ alloy by using electrochemical tests and surface characterization techniques to see their usefulness as dental alloys. Throughout the text, Au_{50}-Ag_{25}-Pd_{25} alloy is referred to as SAAP, while $Ni_{88.6}$-$Cr_{11.4}$ alloy as SNC.

Experimental

Specimens

The conventional arc-melting method was used to prepare the samples SAAP and SNC with the inert atmosphere of pure argon (Ar). The alloys' constituents were weighed and washed with alcohol in an ultrasonic bath and dried in open air prior to the arc melting procedure. The alloy ingot obtained after melting was re-melted 10 times to ensure the homogeneity of alloy components [15]. Samples were cropped into the circular form of diameter of 10 mm, thickness of 2 mm and the exposed surface area was 0.79 cm^2. Before electrochemical testing, the alloys were polished with a carborundum sheet and then bathed with an ultrasonic bath for 10 min in acetone to remove impurities from the surface. One side of both samples was soldered with a copper wire in order to make an electrical connection with the potentiostat [16-18].

Test solution

Fusayama artificial saliva was selected as an electrolyte with the following composition: 0.35 g L^{-1} NaCl, 0.35 g L^{-1} KCl, 0.0906 g L^{-1} $CaCl_2{\cdot}H_2O$, 0.70 g L^{-1} $NaH_2PO_4{\cdot}2H_2O$, 0.05 g L^{-1} $Na_2S{\cdot}9H_2O$ and 1.0 g L^{-1} urea. These constituents were soluble in purified water, and the pH value was adjusted up to 6.5 by using lactic acid [13,14,19].

Corrosion monitoring

Electrochemical tests were performed using a Gamry 3000 potentiostat and a three-electrode setup. The alloy samples served as working electrode(s), while a standard calomel electrode (SCE) was used as the reference electrode and a graphite rod as the counter electrode. Samples were stabilized for 3600 s under open circuit conditions and open circuit potential (OCP) values were measured as a function of time. Electrochemical impedance spectroscopy (EIS) was performed in the frequency range of 100000 to 0.01 Hz with 5 mV sinusoidal voltage. The data were fitted by Gamry Echem analyst software, version 5.30. The results of EIS are shown through Nyquist plots and Bode plots.

The potentiodynamic polarization curves were obtained by scanning the potential from -1 to +1 V with respect to SCE at a scanning rate of 1 mV s^{-1}, corrosion potential (E_{corr}), corrosion current (i_{corr}),

anodic Tafel slope (β_a), and cathodic Tafel slope (β_c) were determined by using extrapolation method [20,21]. Corrosion current densities and corrosion rates were calculated from i_{corr} values.

Surface analysis

The surface analysis of testing samples was carried out through scanning electron microscopy (SEM), linked with energy dispersive spectra (EDS) for the purpose of detecting different elements. The protective oxide film formed on the surfaces of the sample was estimated by images obtained by SEM [18].

Results and discussion

Open circuit potential (OCP)

In corrosion studies, OCP is a crucial parameter that determines the stability of alloy samples in the electrolyte. The behaviour of the oxide film on the surface of the sample is directly related to the variations observed in OCP. The OCP was measured as a function of time for both samples in artificial saliva, and the results are presented in Figure 1 [13].

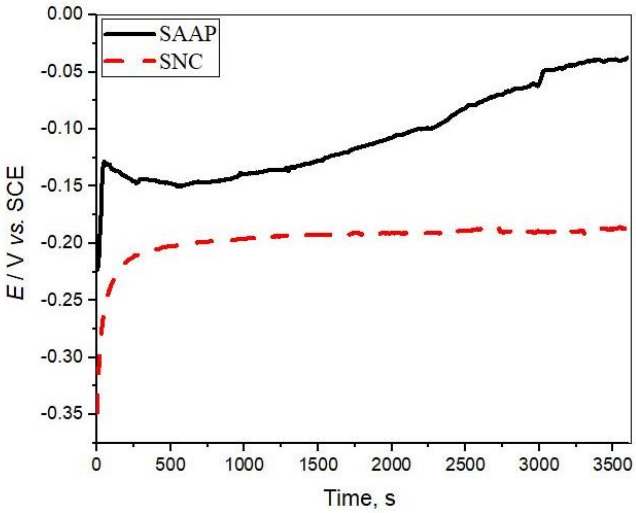

Figure 1. *Open circuit potential vs. time trends of SAAP and SNC samples in artificial saliva*

The experimental results demonstrate a clear increasing trend in OCP values for both samples as a function of time. However, Figure 1 shows that the stability time of the SNC sample was 600 s and that of SAAP sample was 3600 s, suggesting the different behaviour of the two samples. The shift in OCP values towards the positive side indicates the formation of a protective layer for both samples, which is consistent with previous studies [13,16]. For the SAAP sample, the open circuit potential is shifting to more positive values than for the SNC sample during the entire exposure time, which can be explained by an oxide layer at the sample-electrolyte interface, which significantly protects the sample against the aggressiveness of chloride ions from the electrolyte, and results by a low tendency towards corrosion [22,23].

Electrochemical impedance spectroscopy (EIS)

The electrochemical impedance spectroscopy was performed to investigate the corrosion resistance of alloys in artificial saliva at 37 °C. The results of EIS were graphically described by Nyquist and Bode plots shown in Figure 2. Nyquist plots (Z_{imag} *vs*. Z_{real}) of SAAP and SNC samples shown in Figure 2a have similar shapes, with semicircles covering almost all frequency scales. Since charge-transfer resistance is related to the semicircle diameter, an increase in the radius of a semicircle

suggests higher R_{ct} and, thus, a more protective oxide film formed on a sample. Figure 2a shows that SNC has a considerably smaller diameter than the SAAP sample, which suggests that the protection of the oxide film formed on the SAAP sample is stronger than on the SNC sample [13,19].

Bode plots (log modulus $|Z|$ and phase angle *vs*. log of frequency) give more details about the capacitive, inductive, and resistive behaviors of samples at various ranges of frequencies. Bode magnitude plots presented in Figure 2b show that at all frequencies, the SAAP sample possesses a greater modulus of impedance than SNC, thus showing a better protective behaviour of oxide film. Furthermore, it was observed that at the highest frequencies, log $|Z|$ showed a zero-sloping line characteristic for the electrolyte solution resistive response. At other frequencies, the impedance modulus exhibited a near -1 sloping line, suggesting domination of capacitive impedance response in the impedance spectrum. The corresponding Bode phase angle responses in Figure 2b show three different features, *i.e.,* 0° at the highest frequencies, then an increase to higher (negative) values, attaining a maximum close to -68 and -52° for SAAP and SNC samples respectively, and decrease back toward 0° in the low-frequency region.

Such Bode plots (Figure 2b) and single semicircle responses in the Nyquist plot (Figure 2a) are typical for a corrosion process showing resistance R_{ct} and double layer and/or oxide film capacitive response. As stated above, higher semicircle diameter and higher impedance modulus values observed for SAAP indicate that the SAAP sample has stronger corrosion resistance compared to the SNC sample [24].

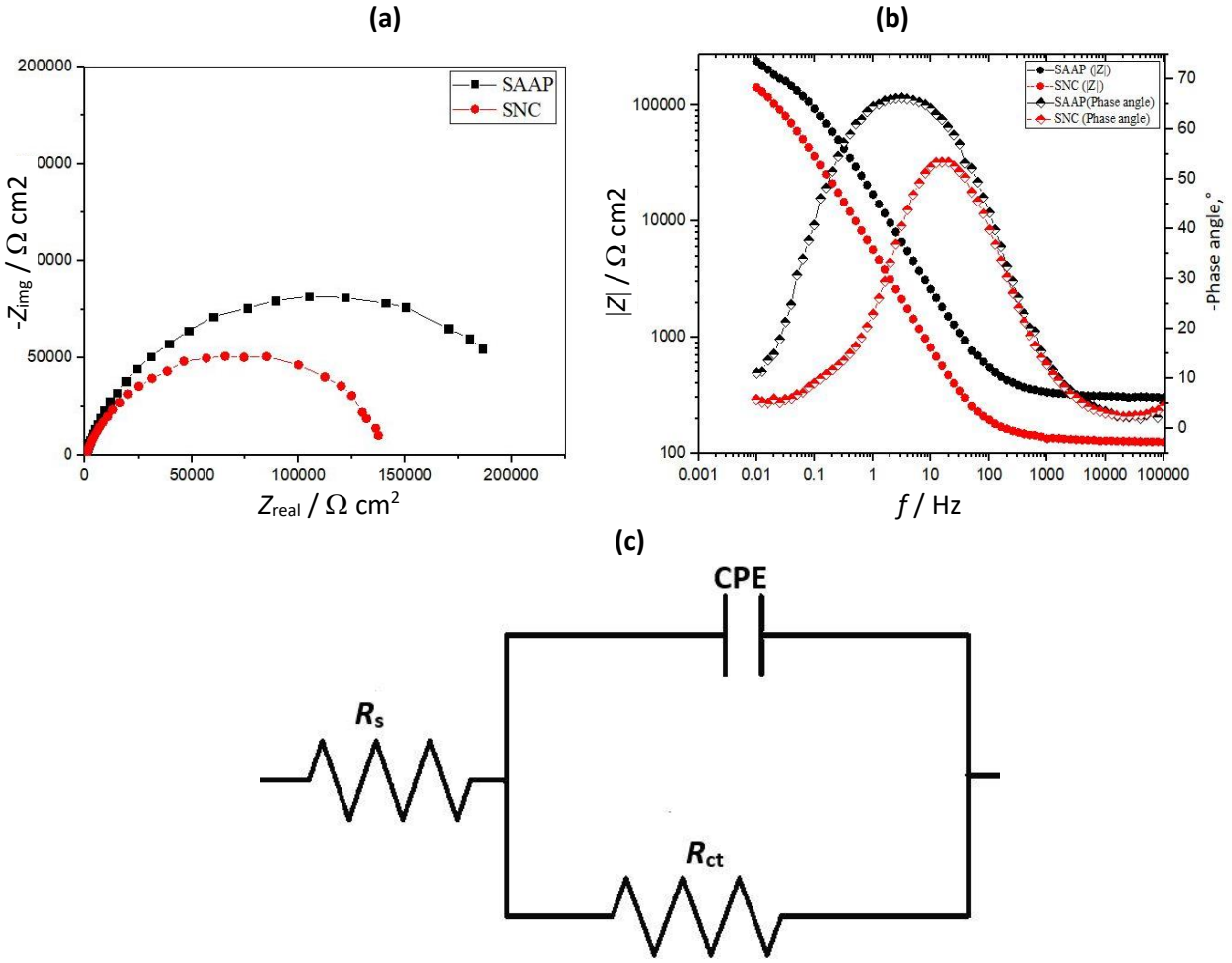

Figure 2. *EIS results for SAAP and SNC samples: (a) Nyquist plots; (b) Bode plots; (c) equivalent electrical circuit (EEC) model*

The most suitable equivalent electrical circuit (EEC) for fitting EIS spectra of samples was the Randles model shown in Figure 2c. In EEC, R_s is a solution resistance, R_{ct} is a charge transfer resistance and CPE is a constant phase element ascribed to oxide film/double-layer capacity. The double-layer capacitor (C_{dl}) was replaced in the Randles equivalent circuit with the constant phase element (CPE) to ensure a more accurate fit. It was calculated by equation (1).

$$C_{dl} = (Y_o R_{ct}^{1-n})^{1/n} \quad (1)$$

In the above equation, Y_0 is the magnitude of the constant phase element (CPE), and n is the exponent, usually in the order of 0 to 1 and provides information regarding the roughness of the surface of samples. If the value of n is −1, 0, and 1, the CPE represents an inductor, resistor, and capacitor, respectively. In this study, n values are between 0.79 and 0.85. The decrease in the value of C_{dl} for the SAAP sample compared to the SNC sample (Table 1) could be attributed to increasing the thickness of the protective layer, which suggests a higher corrosion resistance.

EIS results are given in Table 1. A sample with a higher R_{ct} value exhibits a lower corrosion rate because of the lower release rate of ions into the fluid. The R_{ct} value of the SAAP sample was higher than that of SNC because of the development of a more protective oxide film on its surface, which shows a higher corrosion resistance [14,20,25-27].

Table 1. *EIS parameters of samples SAAP and SNC*

Sample	R_{ct} / kΩ cm^2	R_s / Ω cm^2	n	Y_o / 10^{-5} Ω^{-1} s^n cm^{-2}	C_{dl} / μF cm^{-2}
SAAP	229.8	314.8	0.785	1.26	8.29
SNC	145.7	129.9	0.84	3.78	12.77

Potentiodynamic polarization

The corrosion behavior of samples was investigated using potentiodynamic polarization curves shown in Figure 3. By extrapolating method, the corrosion potential (E_{corr} / V), corrosion current density (j_{corr} / μA cm^{-2}), and the anodic/cathodic (β_a, β_c / V decade^{-1}) parameters might be calculated. The corresponding corrosion rate was calculated using Equation 2 [28]. All calculated parameters are given in Table 2.

$$CR = K_i (j_{corr} / \rho) EW \quad (2)$$

where CR is corrosion rate in mm year^{-1}, K_i= 3.27×10^{-3}, ρ is density in g cm^{-3}, and EW is the equivalent weight of sample material.

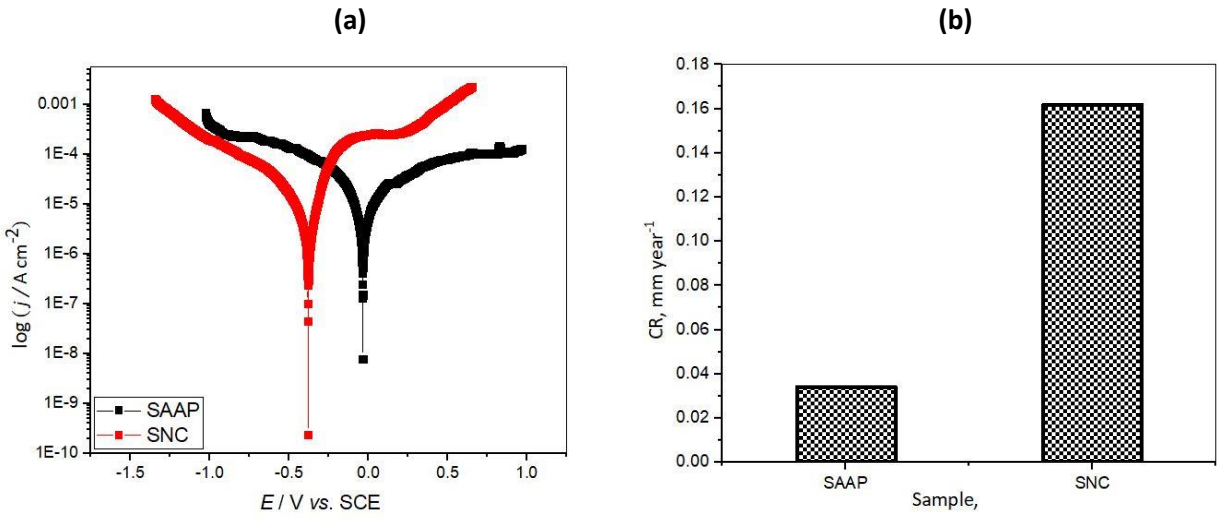

Figure 3. *(a) Potentiodynamic polarization curve for SAAP and SNC samples, (b) corrosion rate*

A low value of j_{corr} represents the formation of a strong oxide layer on metallic surfaces that offers a higher value of corrosion resistance by yielding a lower susceptibility to corrosion mechanisms. It is seen in Table 2 that SNC possesses a higher value of j_{corr} which suggests a smaller value of corrosion resistance by yielding a higher value of corrosion rate compared to the SAAP sample. In terms of corrosion potential (E_{corr}), a more electropositive value shows that a more protective oxide layer has developed on the surface of the sample and indicates a lower corrosion rate. Based on this standard, the SAAP sample with a higher E_{corr} value shows a lower corrosion rate than SNC as shown in Figure 3b [29].

Table 2. *Potentiodynamic polarization parameters for SAAP and SNC samples*

Sample	j_{corr} / µA cm^{-2}	E_{corr} / mV	β_a / mV dec^{-1}	β_c / mV dec^{-1}	CR, mm year^{-1}
SAAP	1.32	-190	321	412	0.034
SNC	2.82	-325	240	320	0.162

Surface characterization of corroded alloys

The surface morphology of both samples was studied by scanning electron microscope (SEM) after performing corrosion testing in artificial saliva. Smaller pores and fewer dark areas could be seen on the SAAP sample compared to SNC, indicating the development of a more protective oxide film and stronger corrosion resistance. On the other hand, continuous propagation of pores and breaking of the oxide film indicate a steady decrease in corrosion resistance. SEM micrographs in Figure 4 reveal the minor-sized pores, major-sized pores, isolated pores, and correlated porous structures. In our study, the average size of the major pores of the samples was measured through Image J software and determined as 13 µm and 60 µm for SAAP and SNC alloys, respectively [30,31].

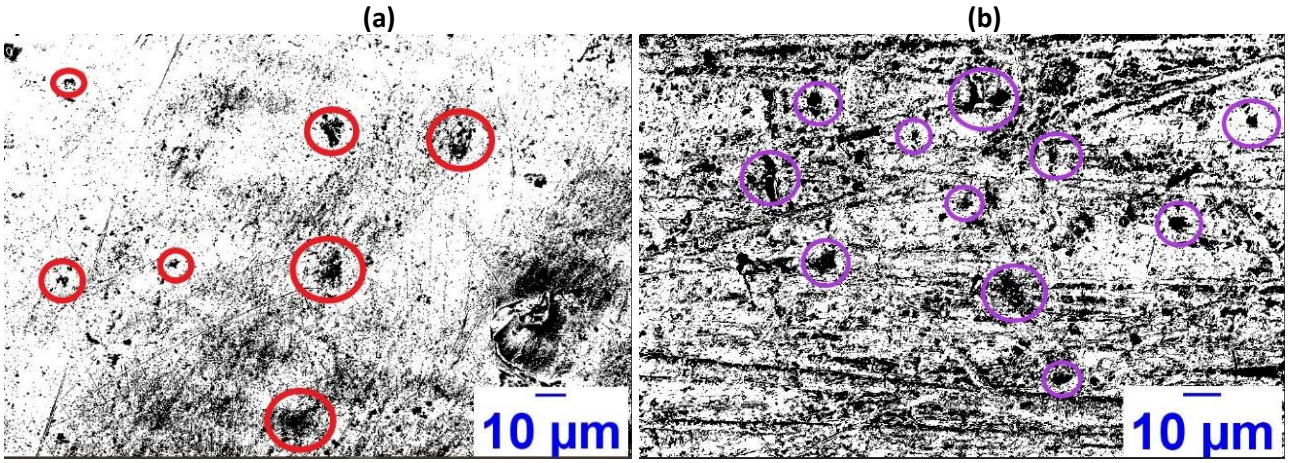

Figure 4. *SEM images at magnification of 100 000× of: (a) SAAP sample; b) SNC sample*

Compositional analysis with EDS

EDS analysis was performed to reveal the chemical composition of the samples. The results obtained are given in Table 3. The presence of oxygen on the surface of the investigated alloys leads to the formation of a protective oxide layer, which protects the samples from corrosion attacks. In the case of the SAAP sample, a protective oxide layer of Ag_2O is formed, but in the case of SNC, oxygen reacts with chromium to form a chromium oxide (Cr_2O_3) layer. As shown in Figure 5, the higher amount of oxygen content and the formation of oxides on the surface of the SAAP sample offers strong corrosion resistance compared to SNC [32]. A high amount of carbon is present in the composition of the sample SAAP, it may be coming from the solder wires.

Table 3. *Results of compositional analysis of sample surfaces by EDS*

Sample	Content, at.%							
	O	Au	Ag	Pd	C	Ni	Cr	Total
SAAP	24.75	19.56	9.31	11.11	35.27	-	-	100
SNC	12.62	-	-	-		76.26	11.12	100

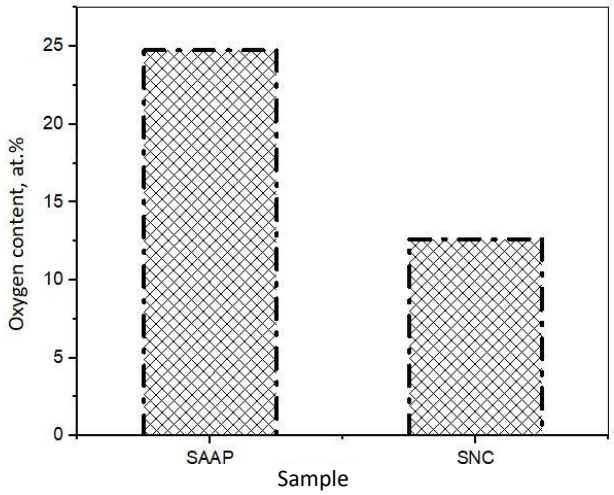

Figure 5*. Histogram showing the amount of oxygen detected on the surface of SAAP and SNC samples*

Conclusions

In this study, $Ni_{88.6}$-$Cr_{11.4}$ and Au_{50}-Ag_{25}-Pd_{25} samples were immersed in an artificial saliva solution and the corrosion resistance was investigated by electrochemical techniques. The formation of a protective oxide layer was examined by OCP, Tafel plots, and EIS spectra. The obtained results were found complementary and in accordance with the results of SEM and EDXS analysis.

- OCP values for SAAP alloy were higher compared to SNC alloy, suggesting an increase in passive oxide thickness.
- The electrochemical impedance spectroscopy showed that the R_{ct} value was higher and C_{dl} was smaller for SAAP alloy as compared to SNC alloy.
- The polarization curves represented that the E_{corr} shifted to more noble values and the j_{corr} decreased significantly for SAAP alloy as compared to SNC alloy.
- The scanning electron microscopy analysis showed that SAAP alloy has smaller pores (13 μm of average size) and a less dark area compared to SNC alloy (60 μm of average size), indicating the development of a more protective oxide film on the surface of SAAP alloy.
- The energy dispersive spectroscopy analysis reveals that alloy SAAP contains a higher amount of oxygen as compared to alloy SNC, suggesting the development of a more protective oxide layer on the surface of SAAP alloy.
- Alloy SAAP has better corrosion resistance compared to SNC alloy and can be recommended for the favourable treatment of patients with dental prostheses.

Acknowledgements: *One of the authors (I.L) acknowledges Dr. Amer Bashir Ziya from the Institute of Physics, Bahauddin Zakariya University, Multan, for funding and supporting.*

References

[1] F. Golgovici, M. Prodana, F. Ionascu, G. Demetrescu, A Comparative Electrochemical and Morphological Investigation on the Behavior of NiCr and CoCr Dental Alloys at Various Temperatures, *Metals* **11(2)** (2021) 256. https://doi.org/10.3390/met11020256

[2] D. Gheorghe, I. Pencea, I. V. Antoniac, R. N. Turcu, R. N., Investigation of the microstructure, hardness and corrosion resistance of a new 58Ag24Pd11Cu2Au2Zn1. 5In1. 5Sn dental alloy, *Materials* **12(4)** (2019) 4199. https://doi.org/10.3390/ma12244199

[3] L. A. O' Brien, R.M. German, Tarnish and corrosion behaviour of palladium-silver alloys, *Journal of Materials Science* **23** (1988) 3563-3571. https://doi.org/10.1007/BF00540496

[4] P. P. Corso, R. M. German, H. D. Simmons, Corrosion evaluation of gold-based dental alloys, *Journal of Dental Research* **64(5)** (1985) 854-859. https://doi.org/10.1177/00220345850640051401

[5] M. Nakagawa, S. Matsuya, M. Ohta, Effect of microstructure on the corrosion behaviour of dental gold alloys, *Journal of Materials Science: Materials in Medicine* **3** (1992) 114-118. https://doi.org/10.1007/BF00705278

[6] P. R. Mezger, A. L. H. Stols, M. M. A. Vrijhoel, E. H Greener, Metallurgical aspects and corrosion behavior of yellow low-gold alloys, *Dental Materials* **5** (1989) 350-354. https://doi.org/10.1016/0109-5641(89)90129-2

[7] H. Herø, Tarnishing in vivo and in vitro of a low-gold alloy related to its structure, *Journal of Dental Research* **6** (1984) 926-931. https://doi.org/10.1177/00220345850640020901

[8] F. Bechir, S. M. Bataga, E. Ungureanu, D. M. Vranceanu, M. Pacurar, E. S. Bechir, C. M. Cotrut, Experimental study regarding the behavior at different pH of two types of Co-Cr alloys used for prosthetic restorations, *Materials* **14(16)** (2021) 4635.https://doi.org/10.3390/ma14164635

[9] L. Niemi, H. Herø, Materials Science Structure, Corrosion, and Tarnishing of Ag-Pd-Cu Alloys, *Journal of Dental Research* **9** (1985) 1163-1169**.** https://doi.org/10.1177/00220345850640091501

[10] M. L. Santos, H. A. Acciari, L. C. O. Vercik, A. C. Guastaldi, Laser weld: microstructure and corrosion study of Ag–Pd–Au–Cu alloy of the dental application, *Materials Letters* **57** (2003) 1888-1893. https://doi.org/10.1016/S0167-577X(02)01095-9

[11] K. Mouflih, K. E. Mouaden, M. Boudalia, A. Bellaouchou, M. Tabyaoui, A. Guenbour, I. Warrad, A. Zarrouk, The Effect of the Moroccan Salvadora Persica Extract on the Corrosion Behavior of the Ni–Cr Non-precious Dental Alloy in Artificial Saliva, *Journal of Bio-and Tribo-Corrosion* **7** (2021) 61. https://doi.org/10.1007/s40735-021-00495-7

[12] L. Porojan, C. E. Savencu, L. V. Costea, M. L. Dan, S. D. Porojan, Corrosion behavior of Ni-Cr dental casting alloys, *International Journal of Electrochemical Science* **13** (2018) 410-423. https://doi.org/10.20964/2018.01.08

[13] G. L. Turdean, A. Craciun, D. Popa, M. Constantiniuc, Study of electrochemical corrosion of biocompatible Co-Cr and Ni-Cr dental alloys in artificial saliva. Influence of pH ofthe solution, *Materials Chemistry and Physics* **233** (2019) 390-398. https://doi.org/10.1016/j.matchemphys.2019.05.041

[14] A. B. Ziya, K. Ohshima, X-ray diffraction study of the structure and thermal parameters of the ternary Au–Ag–Pd alloys, *Journal of Alloys and Compounds* **425** (2006) 123-128. https://doi.org/10.1016/j.jallcom.2006.01.023

[15] C. E. Savencu, L. V. Costea, M. L. Dan, L. Porojan, Corrosion behaviour of Co-Cr dental alloys processed by alternative CAD/CAM technologies in artificial saliva solutions, *International Journal of Electrochemical Science* **13** (2018) 3588-3600. https://doi.org/10.20964/2018.04.40

[16] M. C. Lucchetti, G. Fratto, F. Valeriani, E. De Vittori, S. Giampaoli, P. Papetti, V. R. Spica, L. Manzon, Cobalt-chromium alloys in dentistry: An evaluation of metal ion release, *The Journal of Prosthetic Dentistry* **114** (2015) 602-608. https://doi.org/10.1016/j.prosdent.2015.03.002

[17] J. N. Balaraju, V. Ezhil Selvi, K. S. Rajam, Electrochemical behavior of nanocrystalline Ni–P alloys containing tin and tungsten, *Protection of Metals and Physical Chemistry of Surfaces* **46** (2010) 686-691. https://doi.org/10.1134/S2070205110060109

[18] C. Yang, Q. Wang, Y. Ren, D. Jin, D. Liu, M. Moradi, X. Chen, H. Li, D. Xu, F. Wang, Corrosion behavior of high nitrogen nickel-free austenitic stainless steel in the presence of artificial saliva and Streptococcus mutans, *Bioelectrochemistry* **142** (2021) 107940. https://doi.org/10.1016/j.bioelechem.2021.107940

[19] D. Barjaktarević, J. Bajat, I. Cvijović-Alagić, I. Dimić, A. Hohenwarter, V. Đokić, M. Rakin, The corrosion resistance in artificial saliva of titanium and Ti-13Nb-13Zr alloy processed by high pressure torsion, *Procedia Structural Integrity* **13** (2018) 1834-1839. https://doi.org/10.1016/j.prostr.2018.12.332

[20] M. Bahraminasab, M. Bozorg, S. Ghaffari, F. Kavakebian, Electrochemical corrosion of Ti-Al_2O_3 biocomposites in Ringer's solution, *Journal of Alloys and Compounds* **777** (2019) 34-43. https://doi.org/10.1016/j.jallcom.2018.09.313
[21] X. Z. Xin, J. Chen, N. Xiang, Y. Gong, B. Wei, Surface characteristics and corrosion properties of selective laser melted Co–Cr dental alloy after porcelain firing, *Dental Materials* **30** (2014) 263-270. https://doi.org/10.1016/j.dental.2013.11.013
[22] L. Jinlong, L. Hongyun, Effect of surface burnishing on texture and corrosion behavior of 2024 aluminum alloy, *Surface and Coatings Technology* **235** (2013) 513-520. https://doi.org/10.1016/j.surfcoat.2013.07.071
[23] Y. Lu, S. Guo, Y. Yang, Y. Liu, Y. Zhou, S. Wu, C. Zhao, J. Lin. Effect of thermal treatment and fluoride ions on the electrochemical corrosion behavior of selective laser melted CoCrW alloy, *Journal of Alloy and Compounds* **730** (2018) 552-562. https://doi.org/10.1016/j.jallcom.2017.09.318
[24] Y. Liu, J. Wen, H. Yao, J. He, H.Li, Enhancing the Corrosion Resistance Performance of Mg-1.8 Zn-1.74 Gd-0.5 Y-0.4 Zr, Biomaterial via Solution Treatment Process, *Materials* **13** (2020) 836. https://doi.org/10.3390/ma13040836
[25] Z. Hamidi, S.Y. Mosavian, N. Sabbaghi, M. A. Karimi, M. Noroozifar, Cross-linked poly (N-alkyl-4-vinylpyridinium) iodides as new eco-friendly inhibitors for corrosion study of St-37 steel in 1 M H_2SO_4, *Iranian Polymer Journal* **29** (2020) 225-239. https://doi.org/10.1007/s13726-020-00787-8
[26] M.J. Shivaram, S.B. Arya, J. Nayak, B.B. Panigrahi, Tribocorrosion behaviour of biomedical porous Ti–20Nb–5Ag alloy in simulated body fluid, *Journal of Bio-and Tribo-Corrosion* **7** (2021) 59. https://doi.org/10.1007/s40735-021-00491-x
[27] E. D. Akpan, I. O. Isaac, L. O. Olasunkanmi, E. E. Ebenso, E. S. M. Sherif, Acridine-based thiosemicarbazones as novel inhibitors of mild steel corrosion in 1 M HCl: synthesis, electrochemical, DFT and Monte Carlo simulation studies, *RSC Advances* **9** (2019) 29590-29599. https://doi.org/10.1039/C9RA04778F
[28] D. Mareci, D. Sutiman, A. Cailean, G. Bolat, Comparative corrosion study of Ag-Pd and Co-Cr alloys used in dental applications, *Bulletin of Materials Science* **33** (2010) 491-500. https://doi.org/10.1007/s12034-010-0075-z
[29] F. Bechir, S.M. Bataga, A. Tohati, E. Ungureanu, C. M. Cotrut, E. S. Bechir, M, Suciu, D. M. Vranceanu, Evaluation of the behavior of two CAD/CAM fiber-reinforced composite dental materials by immersion tests, *Materials* **14** (2021) 7185. https://doi.org/10.3390/ma14237185
[30] M. J. Shivaram, S. B. Arya, J. Nayak, B. B. Panigrahi, Electrochemical Corrosion and Impedance Studies of Porous Ti–x Nb–Ag Alloy in Physiological Solution, *Transactions of the Indian Institute of Metals* **73** (2020) 921-928. https://doi.org/10.1007/s12666-020-01904-0
[31] W. Xu, X. Lu, B. Zhang, C. Liu, S. Lv, S. Yang, X. Qu, Effects of porosity on mechanical properties and corrosion resistances of PM-fabricated porous Ti-10Mo alloy, *Metals* **8** (2018) 188. https://doi.org/10.3390/met8030188
[32] F. Bechir, S.M. Bataga, E. Ungureanu, D. M. Vranceanu, M. Pacurar, E. S. Bechir, C. M. Cotrut, Experimental study regarding the behavior at different pH of two types of Co-Cr alloys used for prosthetic restoration, *Materials* **14** (2021) 4635. https://doi.org/10.3390/ma14164635